ACS NANO

www.acsnano.org

ARTICLE

Capsulated Cellular Nanosponges for the Treatment of Experimental Inflammatory Bowel Disease

Yaou Duan, Edward Zhang, Ronnie H. Fang, Weiwei Gao,* and Liangfang Zhang*

Cite This: *ACS Nano* 2023, 17, 15893−15904

Read Online

ACCESS | Metrics & More | Article Recommendations | Supporting Information

ABSTRACT: **Inflammatory bowel disease (IBD) is a chronic gastrointestinal tract disorder characterized by uncontrolled inflammatory responses to the disrupted intestinal epithelial barrier and gut microbiome dysbiosis. Currently available small-molecule immunosuppressive agents and anticytokine biologics show limited potency, mainly due to the complexity of the inflammatory network involved in IBD. Here, we develop an oral formulation of macrophage membrane-coated nanoparticles capsulated in enteric polymer-coated gelatin capsules (denoted "cp-MΦ-NPs") for IBD treatment. The capsules protect the nanoparticles from gastric degradation and allow for targeted delivery to the colon. At the inflamed colon, cp-MΦ-NPs act as macrophage decoys that bind and neutralize pro-inflammatory cytokines. The in vivo treatment efficacy of cp-MΦ-NPs is tested in a mouse model of dextran sulfate sodium-induced colitis. In both prophylactic and delayed treatment regimens, the oral delivery of cp-MΦ-NPs significantly alleviates IBD severity, reflected by reduced intestinal inflammation and intestinal barrier restoration. Overall, cp-MΦ-NPs provide a biomimetic nanomedicine strategy for the treatment of IBD.**

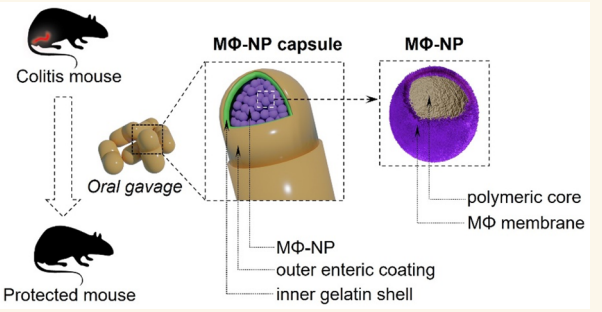

KEYWORDS: *inflammatory bowel disease, gastrointestinal tract, cell membrane coating, nanoparticle, nanomedicine*

Inflammatory bowel disease (IBD) refers to chronic relapsing disorders of the gastrointestinal (GI) tract, including Crohn's disease and ulcerative colitis. These conditions are characterized by intestinal inflammation,[1] intestinal epithelial barrier injury,[2,3] and gut microbiome dysbiosis.[4,5] IBD reduces life quality of patients and places a substantial burden on healthcare systems.[6,7] Current treatments include small-molecule immunosuppressive agents and kinase inhibitors, which can manage symptoms but fail to repair gut mucosal barrier damage or restore intestinal microbiome imbalance.[8] Prolonged use of these nonspecific agents may also lead to severe toxicity and increase the risk of opportunistic infections.[9,10] Alternatively, biologics such as antibodies targeting the tumor necrosis factor (TNF)-α or $\alpha_4\beta_7$ integrin offer promising treatment options for IBD by blocking inflammatory signals. However, these biologics may carry risks of immunogenicity, poor circulation stability, high cost, and antibody resistance upon repetitive administration.[11,12] Therefore, developing effective therapeutics for the IBD is highly desirable.

Recently, nanoparticles have gained considerable attention as potential solutions to the unmet needs of IBD treatment. Nanoparticle delivery systems exhibit attractive characteristics such as target-specificity, stability, biocompatibility, and nontoxicity to the GI system.[13] Various nanoparticle carriers have emerged for the delivery of small-molecular agents, antibodies, and siRNAs to the colon for IBD treatment.[14,15] Some nanoparticles possess pH-responsive,[16,17] ROS-responsive,[18−20] or receptor-mediated targeting properties, which can enhance their specificity and efficacy. In addition to serving as drug carriers, nanoparticles made with macrophage modulatory and reactive oxygen species (ROS)-scavenging materials, such as hyaluronic acid and polydopamine, have been developed as therapeutics for IBD with promising outcomes.[13,21−23]

In the past few years, nanoparticles coated with natural cell membranes have become a compelling anti-inflammatory nanomedicine platform. This platform has been named a "cellular nanosponge" because of its ability to absorb and

Received: May 4, 2023
Accepted: August 9, 2023
Published: August 11, 2023

https://doi.org/10.1021/acsnano.3c03959
ACS Nano 2023, 17, 15893−15904

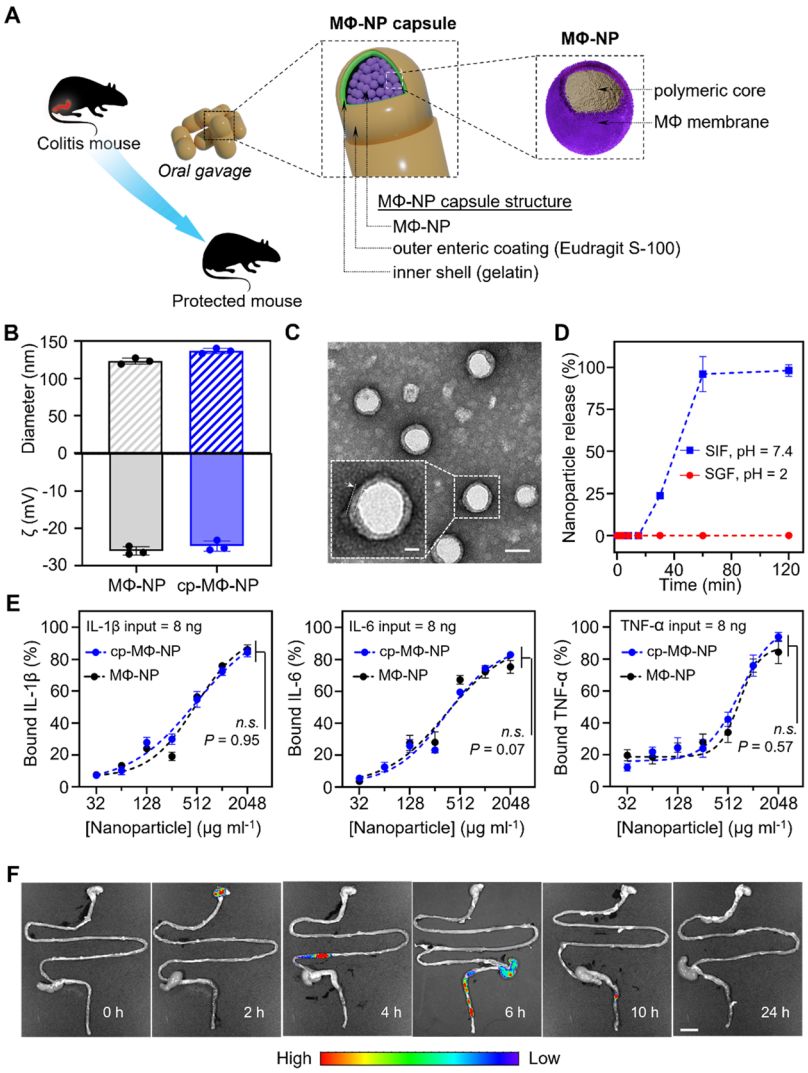

Figure 1. Preparation and characterization of cp-MΦ-NPs. (A) Schematic illustration of cp-MΦ-NPs and their use to manage IBD. MΦ-NP capsules are fabricated by coating MΦ membrane onto polymeric cores, followed by lyophilization, capsule loading, and enteric coating of capsules. (B) The average diameter and surface zeta potential of MΦ-NPs and resuspended cp-MΦ-NPs measured with dynamic light scattering (DLS). (C) Transmission electron microscopy (TEM) images of resuspended cp-MΦ-NPs negatively stained with uranyl acetate. Scale bar = 100 nm (inset scale bar = 30 nm). (D) MΦ-NP release profile from Eudragit S100-coated capsules in simulated gastric fluid (SGF, pH = 2, red) or simulated intestinal fluid (SIF, pH = 7.4, blue). (E) Binding profiles of MΦ-NPs and cp-MΦ-NPs against IL-1β, IL-6, and TNF-α. (F) Representative GI tract images of mice after oral administration of fluorescence-labeled cp-MΦ-NPs. Scale bar = 1 cm. In all data sets, n = 3; data are presented as mean ± s.d.; n.s. = not significant.

neutralize harmful molecules such as toxins and inflammatory cytokines. Among the various types of cellular nanosponges, white blood cell (WBC) nanosponges are made with WBC membranes, which replicate the antigenic profile of the source cell and act as host cell decoys to adsorb inflammatory molecules. WBC nanosponges can effectively bind to different types of cytokines through the corresponding cytokine receptors on the cell membranes.[24] Cytokine neutralization can inhibit downstream macrophage activation and halt the propagation of the immune cascade, thereby reducing inflammation. WBC nanosponges stand out among other anti-inflammatory agents due to their broad-spectrum biological neutralization ability, which is effective against various modes of action of these agents.[24] For example, the use of macrophage membrane-coated nanoparticles (MΦ-NPs) has shown promise in managing sepsis and reducing inflammation in various diseases. These nanoparticles scavenge endotoxins, diverting them away from endogenous macrophages while also neutralizing inflammatory cytokines such as interleukin (IL)-6, IL-1β, and TNF-α. Studies have also demonstrated the efficacy of MΦ-NPs in treating acute pancreatitis and rheumatoid arthritis by inhibiting inflammation and reducing disease severity.[25−27] Following a similar principle, neutrophil nanosponges have also been used to alleviate joint damage in inflammatory arthritis by inhibiting synovial inflammation.[28]

The promise of cellular nanosponges in treating inflammatory disorders has motivated our efforts to investigate their potential use for the treatment of IBD. Here, we report the development of a capsulated oral formulation of MΦ-NPs (denoted "cp-MΦ-NPs") as an effective, safe, and convenient option for IBD treatment. The selection of macrophage membrane over other types of cell membranes is due to the predominant roles of macrophages in IBD pathogenesis.[29] The polymeric core in the MΦ-NP formulation provides a solid

https://doi.org/10.1021/acsnano.3c03959
ACS Nano 2023, 17, 15893−15904

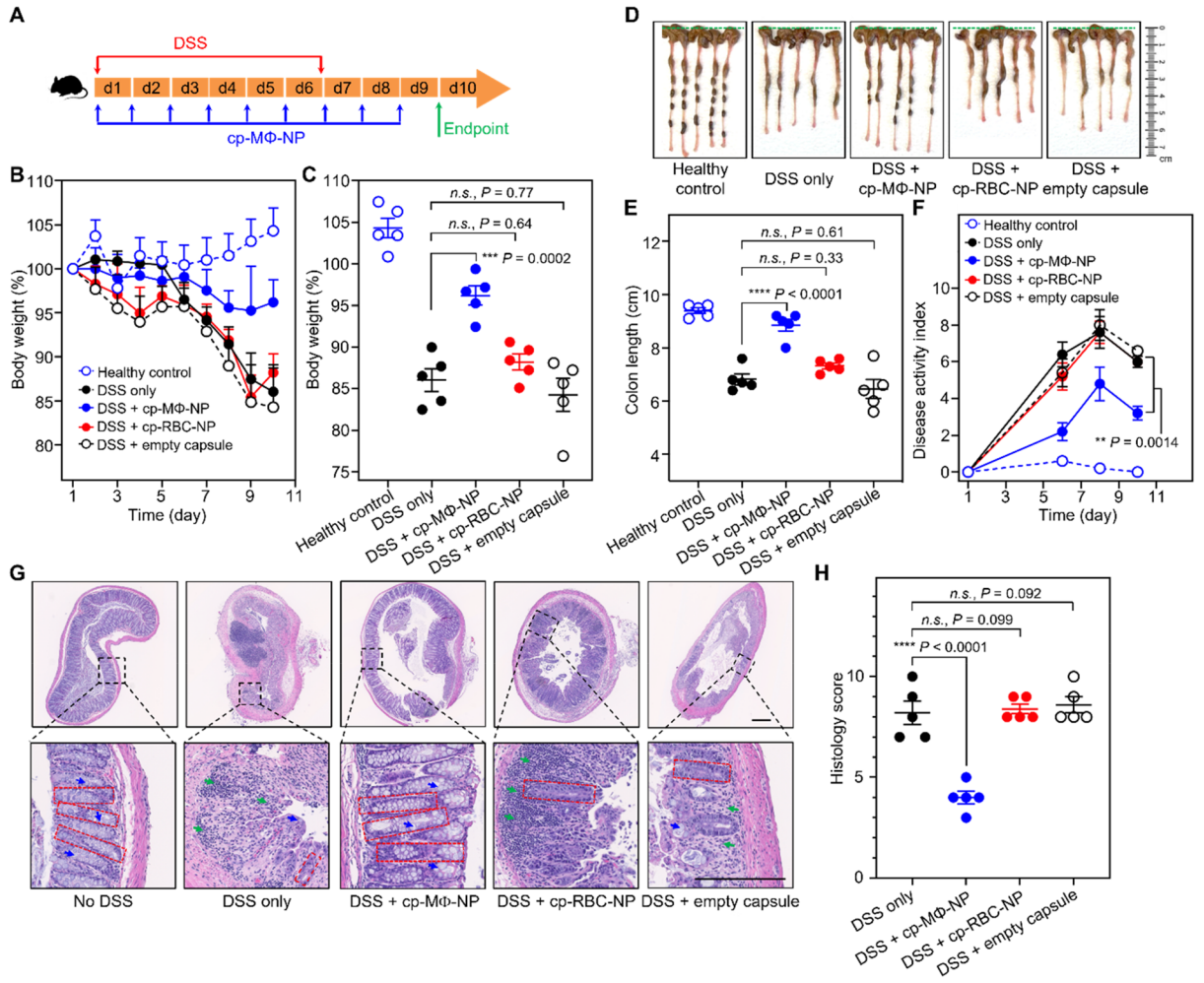

Figure 2. In vivo efficacy of cp-MΦ-NPs for DSS-induced colitis in a prophylactic regimen. (A) The prophylactic study protocol. Seven-week-old male C57BL/6 mice were provided with either water or 3% DSS-containing water for 6 days. Meanwhile, the mice were administrated daily with PBS, an empty capsule, cp-RBC-NPs or cp-MΦ-NPs (3 mg of MΦ-NPs per capsule, 1 capsule per day) via oral gavage for 9 days. (B, C) Daily body weight plotted as the daily value (B) or values at the end of the treatment (C). (D) Mouse colon tissues from different experimental groups were collected and imaged on day 10. (E) Quantification of colon length in (D). (F) The disease activity index (DAI) calculated based on stool consistency (0−4), rectal bleeding (0−4), and weight loss (0−4). (G) Representative H&E staining images of mouse colon tissues from different experimental groups on day 10, scale bar = 1 mm (red dotted box: the crypt, blue arrow: the goblet cell, green arrow: infiltrating immune cells, scale bar in magnified image = 250 μm). (H) Histomorphological evaluation of the colonic damage based on inflammatory cell infiltrate (0−3), epithelial architecture (0−3), muscle thickening (0−3), goblet cell depletion (0−1), and crypt abscess (0−1) as scoring criteria. In all data sets, n = 5; data are presented as mean ± s.d.; n.s. = not significant; ***p < 0.001 and ****p < 0.0001. Statistical analysis was performed with one-way ANOVA.

support of the cell membrane to prevent membrane fusion and maintain nanoparticle stability. A stable MΦ-NP formulation is crucial for accumulation in inflamed colonic epithelium, penetration into the gastrointestinal mucus, and binding with targeted molecules.[21,30,31] We first fabricate MΦ-NPs by coating mouse macrophage membrane onto synthetic cores made from poly(lactic-*co*-glycolic acid) (PLGA). These nanoparticles are then lyophilized and loaded into protective gelatin capsules. The capsules are further dip-coated with pH-responsive enteric polymer coating Eudragit S-100 (Figure 1A). The Eudragit S-100 coated capsules protect cp-MΦ-NPs from the harsh acidic and proteolytic gastric environment and ensure the colonic delivery of the nanoparticles. In vitro, we show that cp-MΦ-NPs can effectively neutralize the inflammatory cytokines associated with IBD. In vivo, we administered cp-MΦ-NPs orally into a mouse model of dextran sulfate sodium (DSS)-induced colitis. Upon release from the capsule in the colon, the released MΦ-NPs mimic endogenous macrophages and bind to pro-inflammatory cytokines that would otherwise target macrophages. As a result, the cp-MΦ-NP treatment restores intestinal barrier functions and ameliorates IBD symptoms in both prophylactic and delayed treatment regimes. Overall, our results suggest that cp-MΦ-NPs are promising biomimetic nanomedicine platforms for the treatment of IBD.

RESULTS AND DISCUSSION

In this study, we formulated cp-MΦ-NPs through a three-step process. First, we fabricated MΦ-NPs through a process including macrophage membrane derivation, PLGA core fabrication, and membrane coating. Second, we suspended the freshly made nanoparticles in 10% sucrose, lyophilized them into a dry powder, and loaded the dry powder into gelatin capsules. The loading was achieved with a special filing

https://doi.org/10.1021/acsnano.3c03959
ACS Nano 2023, 17, 15893−15904

funnel provided by the vendor, and the loading efficiency was 90.8 ± 2.4% (Figure S1). A similar lyophilization process showed to maintain nanosponge size and stability.[32] Third, the capsules were coated with Eudragit S100, a pH-responsive enteric polymer, to ensure colon-specific payload release.[33] Dynamic light scattering (DLS) measurements revealed that resuspended cp-MΦ-NPs and freshly prepared MΦ-NPs had a comparable hydrodynamic diameter (137.0 and 123.7 nm, respectively) and surface zeta potential (−24.8 and −26.1 mV, respectively), suggesting that the lyophilization and encapsulation procedures had negligible impact on the nanoparticle structures (Figure 1B). In addition, cp-MΦ-NPs revealed a characteristic core−shell morphology under transmission electron microscopy (TEM). The morphology is comparable to freshly prepared MΦ-NPs, confirming the preservation of nanoparticle structure during the formulation process (Figure 1C and Figure S2).[34]

To test pH-responsive nanosponge release from the capsules, we labeled cp-MΦ-NPs with a fluorescent dye and placed the capsules in a simulated gastric fluid (SGF, pH = 2). Negligible amounts of MΦ-NPs were released from the capsules into the fluid in 2 h. In contrast, when placed in a simulated intestinal fluid (SIF, pH = 7.4), the capsules released about 90% of the loaded MΦ-NPs within 60 min. This test confirmed a pH-responsive MΦ-NP release from the capsules (Figure 1D). When suspended in SIF (pH = 7.4), the hydrodynamic size of cp-MΦ-NPs remained stable for 7 days, indicating excellent colloidal stability (Figure S3). We also incubated cp-MΦ-NPs released from the capsules with IL-1β, IL-6, and TNF-α, three representative pro-inflammatory cytokines in IBD.[35,36] Nanoparticle binding with these cytokines showed a clear dose dependence of binding kinetics (Figure 1E). In fact, cp-MΦ-NPs and freshly prepared MΦ-NPs showed comparable cytokine binding kinetics and capacity, implying that the cp-MΦ-NP formulation preserved the cytokine binding bioactivity of MΦ-NPs. A Western blot analysis further verified the preservation of key MΦ surface antigens on cp-MΦ-NPs (Figure S4). Moreover, cp-MΦ-NPs were also able to ameliorate the cytokine-induced inflammatory effect on macrophages and the reactive oxygen species (ROS) effect on colon epithelial cells in vitro (Figure S5). Lastly, when tested on MC38 cells, a colon tumor cell line derived from colon epithelial cells, cp-MΦ-NPs showed the absence of cytotoxicity (Figure S6).

To study the specificity of cp-MΦ-NPs for colon delivery, we administered fluorescence-labeled cp-MΦ-NPs orally into C57BL/6 mice and observed their colonic distribution at predetermined time points (Figure 1F). At 2 and 4 h after the oral administration, most cp-MΦ-NPs were at the stomach and the ileum, respectively. The fluorescent signal was confined within a narrow region during this period, suggesting an intact capsule structure. At 6 h, the fluorescence predominantly localized at the colon and its distribution became broader, suggesting the dissolution of the capsule and the release of cp-MΦ-NPs. At 10 h, the nanoparticle fluorescence intensity diminished significantly and became undetectable at 24 h. These results verified that the capsules were able to deliver cp-MΦ-NPs specifically to the colon after oral administration.

Next, we investigated the efficacy of cp-MΦ-NPs to ameliorate IBD in a prophylactic regimen using a mouse model of DSS-induced colitis. Specifically, we provided C57BL/6 mice with drinking water containing 3% DSS for 6 days while administrating cp-MΦ-NPs (3 mg MΦ-NPs per capsule; 1 capsule per day for 9 days) via oral gavage (Figure 2A).[36] The control groups included healthy mice and mice treated with DSS only, DSS with capsulated red blood cell membrane-coated nanoparticles (denoted as "cp-RBC-NPs"), or DSS with empty capsules. We first monitored mouse body weight change among different groups as an efficacy indication.[37] Compared to the healthy controls, the administration of DDS alone led to rapid weight loss in the treated mice (Figure 2B). A maximum weight loss was observed on day 10, which amounted to a decrease to 86% of the original weight (14% loss). This confirmed the establishment of a disease model (Figure 2C). Throughout the study, mice treated with cp-MΦ-NPs showed the smallest body weight loss (retaining over 95% of the original body weight on day 10), indicating effective amelioration of the colitis symptoms. Notably, mice treated with cp-RBC-NPs or empty capsules showed comparable weight loss as that of the DDS-only group (no treatment), of which the body weight reduced to 88% and 84% of the original body weight, respectively.

The colon length of mice with DSS-induced colitis correlates with the disease severity, as more severe colitis corresponds to a shorter colon length.[21,36] Therefore, we used colon length as another indication to evaluate the efficacy of the cp-MΦ-NP treatment. Compared to the colon of healthy mice, the colon of mice with colitis shortened significantly (Figure 2D). In contrast, the colon length of mice treated with cp-MΦ-NPs is comparable to that of the healthy controls. Neither cp-RBC-NPs nor empty capsules showed efficacy. Quantitative colon length measurements further confirmed the above observation. The average colon length of the healthy mice was 9.4 ± 0.2 cm. DSS challenge shortened the colon length to an average of 6.5 ± 0.5 cm. On the contrary, cp-MΦ-NP treatment restored the colon length to 8.8 ± 0.5 cm, comparable to that of healthy mice, and significantly longer than that in either cp-RBC-NP or empty capsules treatment groups (7.3 ± 0.2 cm and 6.5 ± 0.8 cm, respectively) (Figure 2E). In the study, we also monitored the disease activity index (DAI), a summation of weight loss scores, stool consistency scores, and rectal bleeding scores (Table S1).[21,36] As shown in Figure 2F, cp-MΦ-NP treatment significantly decreased the DAI throughout the study as compared to that of DSS-challenged mice and mice treated with cp-RBC-NPs or the empty capsules. We then performed a histological analysis of the colon tissues to investigate the cp-MΦ-NP efficacy at a tissue level. Colon tissue from healthy mice showed well-defined finger-like crypt structures, goblet cells, and the absence of infiltrating immune cells (Figure 2G). Without treatment (DSS only), the colon tissue of the mice with IBD showed heavy crypt distortion, severe goblet cell loss, and noticeable infiltrating immune cells, comparable to previously reported histological analysis.[21] Colon tissue from mice treated with cp-MΦ-NPs showed histological features similar to those of the healthy controls, including regular crypt structures, minimal loss of goblet cells, and a low level of infiltrating immune cells. Meanwhile, colon tissues of mice treated with cp-RBCs-NPs or empty capsules showed distinctive histological features like those in the no-treatment group. We calculated the histology scores summarizing the key colonic damage features.[38] As shown in Figure 2H, the cp-MΦ-NP treatment significantly reduced the scores to a level close to that of the healthy controls. In contrast, all other treatments scored highest, demonstrating cp-MΦ-NP protection against pathological damage in colonic epithelium.

https://doi.org/10.1021/acsnano.3c03959
ACS Nano 2023, 17, 15893−15904

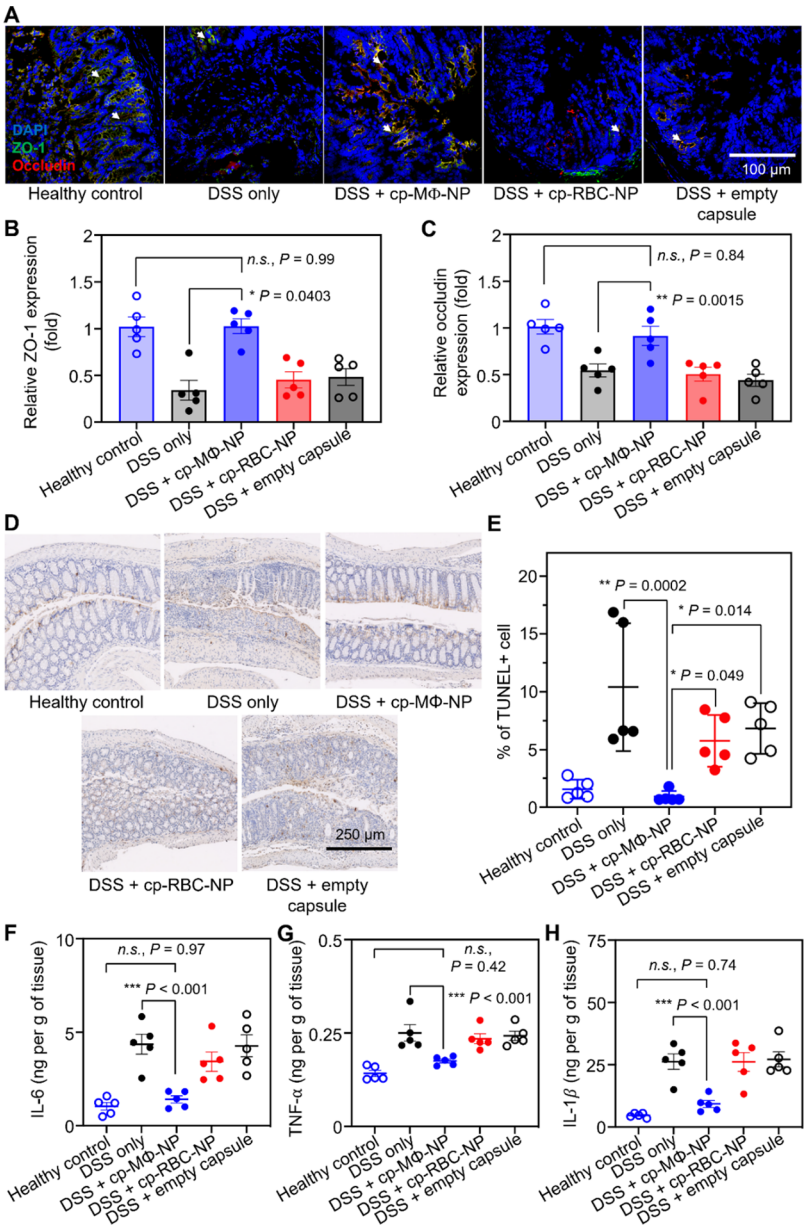

Figure 3. Cellular and molecular studies of cp-MΦ-NPs protecting colonic epithelium. (A) Representative immunofluorescence images of colon sections collected on day 10 after the indicated treatments for analysis of the tight junction ZO-1 and occludin expressions. (B, C) Quantitative mRNA expression levels of ZO-1 (B) and occludin (C) via RT-PCR. (D) Representative TUNEL staining of colon sections collected on day 10 after the indicated treatments. (E) Quantification of TUNEL positivity based on (D). (F–H) Quantitative analysis of the pro-inflammatory cytokine levels, including IL-6 (F), TNF-α (G), and IL-1β (H) on day 10 after the indicated treatment. In all data sets (E–H), n = 5; data are presented as mean ± s.d.; n.s. = not significant; *p < 0.05, **p < 0.01, and ***p < 0.001; statistical analysis was performed with one-way ANOVA.

To evaluate the in vivo cp-MΦ-NP efficacy at a cellular level, we examined the colonic epithelial cell function and barrier integrity at the end of the indicated treatments. Tissue cross sections from the healthy mice stained for zonula occludens protein-1 (ZO-1) and occludin, two signature tight junction-associated proteins, showed strong fluorescence with orderly patterns on the colonic lumen, indicating an intact intestinal barrier (Figure 3A).[21] However, the fluorescence diminished in the cross sections of the tissue from mice with colitis who received no treatment, suggesting disruptions of the colon epithelial and mucosal barriers. The cp-MΦ-NP treatment restored the tissue damage, preserving the colonic epithelial cell function and barrier integrity. Notably, ZO-1 and occludin expressions on samples of mice treated with cp-RBC-NPs and empty capsules appeared similar to those in the DSS group without treatment, indicating the absence of efficacy. To gain a quantitative comparison, we evaluated ZO-1 mRNA (mRNA) expression in intestinal epithelial cells (Figure 3B). Consistent with the protein immunofluorescence analysis, the cp-MΦ-NP treatment kept the expression of ZO-1 mRNA at a level comparable to that of the healthy controls. All other treatment groups showed significant reductions in ZO-1 mRNA expression. We also found similar results when analyzing occludin mRNA expression, where mice treated with cp-MΦ-NPs showed a similar expression level as the healthy mice (Figure 3C).

https://doi.org/10.1021/acsnano.3c03959
ACS Nano 2023, 17, 15893–15904

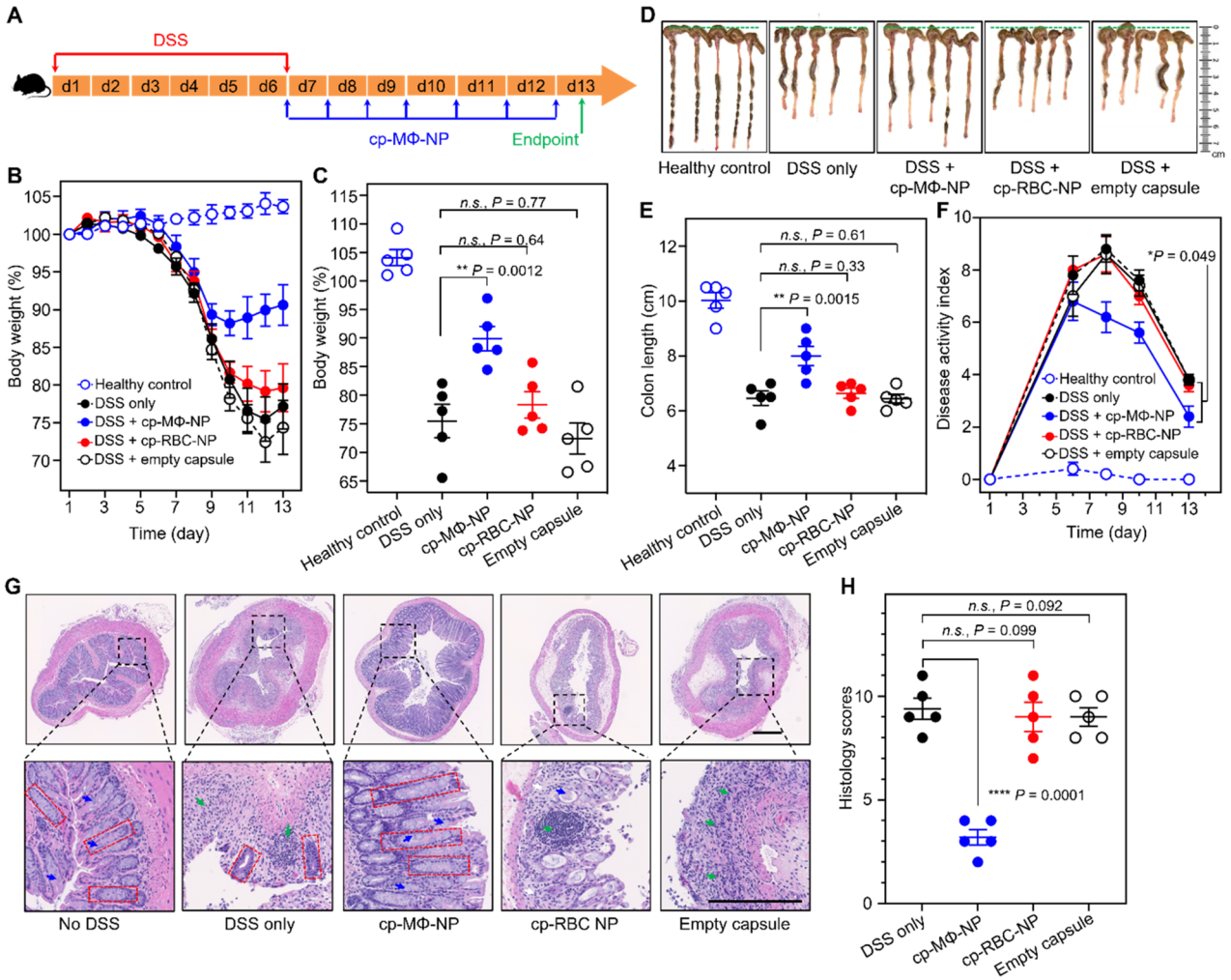

Figure 4. In vivo efficacy of cp-MΦ-NPs for DSS-induced colitis in a delayed treatment regimen. (A) The delayed treatment study protocol. Seven-week-old male C57BL/6 mice were provided with either water or 3% DSS-containing water for 6 days. Then the mice were administrated daily with PBS, an empty capsule, cp-RBC-NPs, or cp-MΦ-NPs (3 mg of MΦ-NPs per capsule; 1 capsule per day) via oral gavage from day 7 to day 13. (B, C) Daily body weight plotted as the daily value (B) or values at the end of the treatment (C). (D) Mouse colon tissues from different experimental groups were collected and imaged on day 13. (E) Quantification of colon length in (D). (F) The disease activity index (DAI) calculated based on stool consistency (0−4), rectal bleeding (0−4), and weight loss (0−4). (G) Representative H&E staining images of mouse colon tissues from different experimental groups on day 13, scale bar = 1 mm (red dotted box: the crypt, blue arrow: the goblet cell, green arrow: infiltrating immune cells, scale bar in magnified image = 250 μm). (H) Histomorphological evaluation of the colonic damage based on inflammatory cell infiltrate (0−3), epithelial architecture (0−3), muscle thickening (0−3), goblet cell depletion (0−1), and crypt abscess (0−1) as scoring criteria. In all data sets, n = 5; data are presented as mean ± s.d.; n.s. = not significant; *p < 0.05, **p < 0.01, and ****p < 0.0001; statistical analysis was performed with one-way ANOVA.

We further evaluated intestinal epithelial cell function via a terminal deoxynucleotidyl transferase dUTP nick end labeling (TUNEL) assay (Figure 3D).[39] Compared to the healthy controls, the TUNEL assay found colonic epithelium apoptosis in large areas of the crypts from mice with DSS-induced colitis. Treatment with cp-MΦ-NPs reduced the apoptosis to a level comparable to that of healthy controls. Groups treated with cp-RBC-NPs or empty capsules showed apoptosis levels comparable to those of the disease group. Further quantification of TUNEL-positive cells is consistent with the observation, confirming the efficacy of cp-MΦ-NPs (Figure 3E). We hypothesize that the observed anti-inflammatory efficacy was due to the capability of cp-MΦ-NPs to neutralize pro-inflammatory cytokines. To test this hypothesis, we measured colonic concentrations of representative pro-inflammatory cytokines, including IL-6, TNF-α, and IL-1β. As shown in Figure 3F, mice pretreated with DSS exhibited a significant increase in colonic IL-6 levels compared to the healthy controls, consistent with previous studies.[21,36] In contrast, the local IL-6 level in mice treated with cp-MΦ-NPs decreased to a comparable level to the healthy controls. Similar results were also observed for TNF-α and IL-1β, confirming the pro-inflammatory cytokine neutralization capability of cp-MΦ-NPs (Figure 3G, H).

To fully evaluate the treatment benefit of cp-MΦ-NPs for IBD, we examined the in vivo efficacy in a delayed treatment regimen where cp-MΦ-NPs were administered after establishing the colitis (Figure 4A). In the study, administration of DDS alone led to significant body weight loss with time. Without treatment, mice with DSS-induced colitis showed a continuous body weight loss with 75.5% of the original body weight on day 13 (Figure 4B). Within the same period, mice treated with cp-MΦ-NPs showed significant body weight recovery, reaching 90% of the original body weights on day 13, indicating a

https://doi.org/10.1021/acsnano.3c03959
ACS Nano 2023, 17, 15893−15904

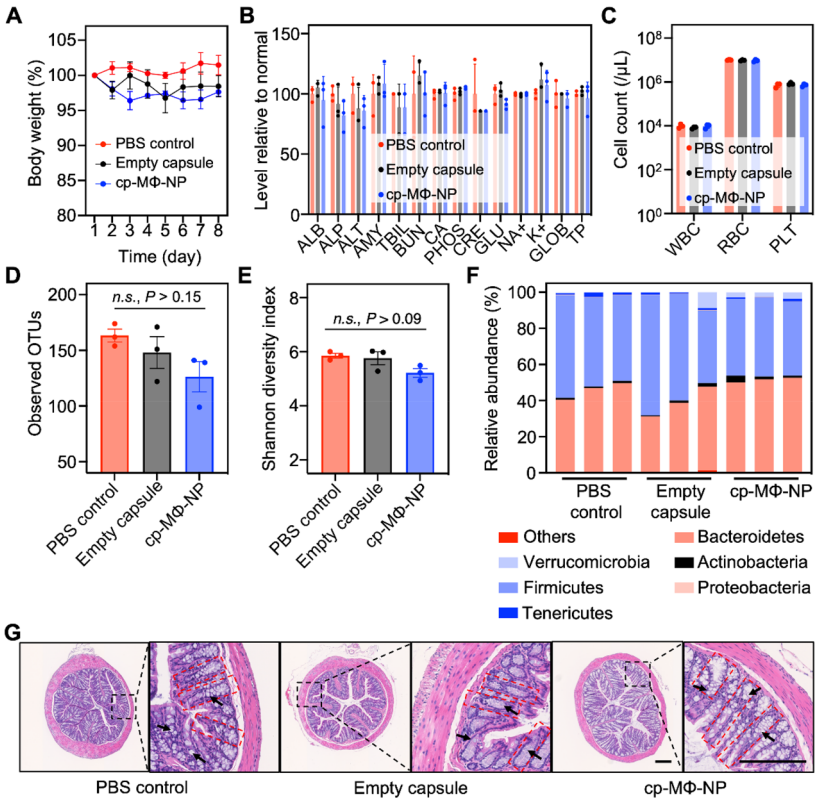

Figure 5. In vivo biosafety analysis of cp-MΦ-NPs. Seven-week-old male C57BL/6 mice were administrated daily with PBS, an empty capsule, or cp-MΦ-NPs (3 mg of MΦ-NPs per capsule; 1 capsule per day) via oral gavage for 7 days. (A) Daily body weight during the study. (B, C) Comprehensive serum chemistry panel (B) and blood cell count (C) performed at the end of the 7-day treatments. ALB, albumin; ALP, alkaline phosphatase; ALT, alanine aminotransferase; AMY, amylase; TBIL, bilirubin; BUN, urea nitrogen; CA, calcium; PHOS, phosphorus; CRE, creatinine; GLU, glucose; NA^+, sodium; K^+, potassium; GLOB, globulin (calculated); TP, total protein. (D, E) Gut microbiome analysis based on quantification of microbial community observed OTU richness (D) and quantification of α-diversity (Shannon index, E). (F) Relative abundance of gut microbiome at phylum-level taxa presented as a percentage of total sequences. (G) H&E-stained histological sections from colonic tissues collected at the end of the 7-day treatments. Red dotted boxes indicate the crypts, and black arrows indicate the goblet cells. Scale bar = 250 μm. In all data sets, n = 3; data are presented as mean ± s.d.; n.s. = not significant.

preclinical treatment benefit of cp-MΦ-NPs. Colitis mice treated with cp-RBC-NPs or empty capsules showed weight loss similar to that of the DSS-only group, confirming the treatment efficacy of cp-MΦ-NPs (Figure 4C). At the study end point, the mice were sacrificed and examined the colon length. The cp-MΦ-NP treatment preserved the colon length comparable to that of the healthy controls (Figure 4D). Neither cp-RBC-NP nor empty capsules showed efficacy. Quantitative measurements of the colon length further confirmed the efficacy observed with cp-MΦ-NPs (Figure 4E). Meanwhile, the DAI values of the mice treated with cp-MΦ-NPs decreased once the treatment started (Figure 4F), but the DAI values of the mice in other groups remained high. Histological analysis showed that the colon tissues from healthy mice displayed well-defined finger-like crypt structures, goblet cells, and no infiltrating immune cells, indicating intact colonic epithelial barriers (Figure 4G). However, the DSS challenge impaired the colonic epithelial barriers, indicated by severe crypt distortion, severe goblet cell loss, and heavy infiltration of immune cells. Colon tissues from mice treated with cp-MΦ-NPs showed histological features similar to those of the healthy controls. In contrast, tissues from mice treated with cp-RBC-NPs or empty capsules exhibited histological features such as the DSS-only group. We also scored the severity of colonic epithelial barrier damage and found mice treated with cp-MΦ-NPs were scored similarly to the healthy controls (Figure 4H). Their scores were significantly lower than those of other treatment groups. Collectively, these results confirmed that cp-MΦ-NPs effectively ameliorated DSS-induced colitis damage in a delayed treatment regimen.

Finally, we evaluated the acute toxicity of cp-MΦ-NPs after their oral administration to healthy C57BL/6 mice. Each mouse received one capsule per day (3 mg of cp-MΦ-NPs per capsule) from day 1 to day 7. Mice administrated with PBS or empty capsules served as controls. We monitored body weight changes daily but found no significant weight loss in all groups (Figure 5A). On day 8, we collected blood, feces, and colons from the mice and performed comprehensive biomarker analyses. Serum metabolic panel analysis showed no significant changes in biomarkers associated with liver or kidney functions in mice treated with cp-MΦ-NPs (Figure 5B). Moreover, the WBCs, RBCs, and platelets remained at levels comparable to those of all groups (Figure 5C).

Analysis of fecal samples via 16S rRNA sequencing in the V3 and V4 regions also demonstrated that daily administration of cp-MΦ-NPs induced an insignificant impact on the operational taxonomic unit (OTU) richness, representing intestinal flora abundance (Figure 5D). Measurements of the Shannon α-diversity index also showed a negligible impact of cp-MΦ-NP treatment on the microbiota richness and distribution evenness (Figure 5E). Examination of the relative abundance of flora at the phylum level exhibited a similar microbiome composition

https://doi.org/10.1021/acsnano.3c03959
ACS Nano 2023, 17, 15893−15904

among all experimental groups (Figure 5F). Furthermore, we collected the colonic tissues and stained the sections with hematoxylin and eosin (H&E) for histopathological analysis (Figure 5G). We found that the overall structure, integrity, and immune infiltration of tissues in mice treated with cp-MΦ-NPs or empty capsules were similar to those of the PBS control group. Together, these results indicate that cp-MΦ-NPs have a high biosafety profile.

CONCLUSIONS

In summary, we have successfully developed a capsulated MΦ-NP formulation that showed great promise as an anti-inflammatory strategy for managing IBD. The resulting cp-MΦ-NPs were able to withstand the harsh gastric environment and deliver the medication directly to the inflamed colon without being denatured. Once at the disease site, the MΦ-NPs were released from the capsules and presented the same antigenic profiles as the endogenous macrophages, acting as decoys to neutralize pro-inflammatory cytokines. Unlike conventional anticytokine biologics that inhibit specific and limited targets, cp-MΦ-NPs represent a broad-spectrum approach that provides a disease-relevant inhibition of the inflammation cascade in IBD. In a DSS-induced murine IBD model, oral administration of cp-MΦ-NPs in both prophylactic and delayed treatment regimens significantly reduced colonic pro-inflammatory cytokine levels. The treatment resulted in body weight recovery, preservation of colon length, and colon tissue protection. Importantly, cp-MΦ-NPs showed no acute toxicity.

In previous studies, cellular nanosponges have shown efficacy in treating various inflammatory diseases.[40,41] The characteristics of these diseases play a crucial role in determining the design of nanosponge formulations. Factors such as the membrane type, the route of administration, and membrane functionalization are typically tailored accordingly. In this work, the development of cp-MΦ-NPs exemplifies the underlying principle of biological neutralization shared by various types of cellular nanosponges. However, the cp-MΦ-NP formulation illustrates the importance of customized design features, including freeze-drying, capsule encapsulation, colon targeting, and oral delivery. The success of this approach has greatly expanded the application potential of the cellular nanosponge platform.

Toward future translation of cp-MΦ-NPs, several critical aspects should be considered. First, optimizing the physicochemical properties of the nanosponges may further enhance the disease-targeting ability and treatment efficacy of cp-MΦ-NPs. For instance, modifying the surface chemistry of the nanosponges can reduce absorption by healthy tissue while enabling deeper penetration into inflamed tissue, thereby enhancing their anti-inflammatory activity.[42] Tuning the size and size distribution of the nanosponges may also improve nanoparticle diffusion and retention, leading to better treatment efficacy. Additionally, robust evidence in mouse models suggests that an altered intestinal microbial flora may contribute to IBD development and progression.[43,44] Thus, modulating interactions of nanosponges with microbiota and infiltrated immune cells could be beneficial. Nanosponge surface functionalization approaches, such as lipid insertion, membrane hybridization, metabolic synthesis, and genetic engineering, can help achieve this goal. Furthermore, it is crucial to establish a large-scale manufacturing process along with adequate quality control and quality assurance measures to ensure an adequate supply of cp-MΦ-NPs for preclinical and clinical tests. These challenges and opportunities remain to be explored in the future.

METHODS

Macrophage Membrane Derivation. The cell membrane of J774 cells, a mouse macrophage cell line, was collected according to a previously established protocol.[25] Briefly, frozen cell stocks were thawed and washed with 1× phosphate-buffered saline (PBS, Corning) three times. Cells were then suspended in a hypotonic lysing buffer containing 30 mM Tris-HCl (pH 7.5), 225 mM D-mannitol, 75 mM sucrose, 0.2 mM ethylene glycol-bis(β-aminoethyl ether)-*N*,*N*,*N*′,*N*′-tetraacetic acid) (EGTA, all from Millipore-Sigma), and a protease and phosphatase inhibitor cocktail (Thermo Fisher Scientific). After 15 min of incubation at room temperature, cells were disrupted using a Dounce homogenizer with a tight-fitting pestle (20 passes). The homogenized solution was centrifuged at 10,000*g* for 25 min at 4 °C. The pellets were discarded, and the supernatant was centrifuged again at 150,000*g* for 35 min at 4 °C to pellet the membrane. Following the centrifugation, the membrane was washed once by being resuspended in ethylenediaminetetraacetic acid (EDTA, 37 mL, 0.2 mM, Millipore-Sigma) and collected with centrifugation at 150,000*g* for 35 min at 4 °C. Finally, the membrane was resuspended in 1 mL of 0.2 mM EDTA. The membrane protein concentration was measured by using a BCA kit (Pierce Thermo Scientific). The membrane suspension was stored at −80 °C for subsequent uses.

Red Blood Cell (RBC) Membrane Derivation. Human RBC membrane derivation was performed using a published protocol.[45,46] Briefly, packed human RBCs (ZenBio Inc.) were washed with ice-cold 1× PBS and lysed with a hypotonic solution containing 0.25× PBS for 20 min. After the cell lysing process, the lysed cells were pelleted by centrifugation at 800*g* for 5 min, followed by removal of the supernatant containing hemoglobin. Such hypotonic-based cell lysing steps were repeated three times. The RBC membrane was resuspended in water at a protein concentration of 10 mg mL^{-1} and stored at −80 °C for subsequent studies.

Preparation of Cell Membrane-Coated Nanoparticles. Nanoparticles coated with J774 mouse macrophage membrane (denoted "MΦ-NPs") were synthesized using a previously published procedure.[25] Briefly, 1 mL of poly(DL-lactic-*co*-glycolic acid) (PLGA, 50:50, 0.67 dL g^{-1}, Lactel Absorbable Polymers) in acetone (20 mg mL^{-1}, Millipore-Sigma) was added dropwise into 4 mL water. The mixture was vacuumed under an aspirator for 2 h to evaporate the acetone completely. For fluorescence imaging, 1,1′-dioctadecyl-3,3,3′,3′-Tetramethylindotricarbocyanine Iodide (DiR, excitation/emission = 748/780 nm, Thermo Fisher Scientific) was added to the PLGA solution before the mixture was added into the water. The dye concentration was 0.1 wt % of PLGA polymer. The macrophage membrane was mixed with the PLGA core for cell membrane coating at a polymer-to-membrane protein weight ratio of 1:1. The mixture was then sonicated with a bath sonicator (Fisher Scientific FS30D) for 3 min. RBC membrane-coated nanoparticles (denoted "RBC-NPs") were fabricated following the same process.

Preparation of Nanoparticle-Loaded Capsules. For MΦ-NP encapsulation, MΦ-NPs were first lyophilized in 10% sucrose for 48 h using a FreeZone 4.5 lyophilizer (Labconco). Following the lyophilization, 3 mg of MΦ-NP powder was loaded into a mouse-specific, size M gel capsule using a capsule loading kit (all from Braintree Scientific). After encapsulation, capsules were coated with the commercial enteric coating polymer Eudragit S100 (Evonik Operations) for protection from the gastric environment. In brief, the Eudragit S100 polymer was dissolved in 95% ethanol (Koptec) with 2.5% triethyl citrate (Millipore-Sigma) to a final concentration of 6 w/v%. The polymer solution was then stirred overnight in a closed container at room temperature. The capsules were dipped into the Eudragit S100 coating solution for coating, followed by 25 min of air-dry. The dip-coating process was repeated three times. Loading RBC-NP into the capsules was performed by following the same procedure.

https://doi.org/10.1021/acsnano.3c03959
ACS Nano 2023, 17, 15893−15904

Nanoparticle Physicochemical Characterization. The size (diameter, nm) and surface zeta potential (mV) of the nanoparticles were measured by using dynamic light scattering (DLS, Malvern Zetasizer Nano ZS). For studying morphology, the nanoparticle samples were adsorbed onto carbon-coated copper grids (400-mesh, Electron Microscopy Sciences) and stained with 0.2 wt % uranyl acetate (Electron Microscopy Sciences). The grids were imaged on a JEOL 1200 EX II transmission electron microscope. For evaluating the colloidal stability, the samples were incubated in SIF at 37 °C, and the nanoparticle size was measured daily with DLS for 7 days. For evaluating the protective effect of the capsule against the gastric environment, DiD-labeled MΦ-NPs were lyophilized and loaded into Eudragit S100-coated capsules. Then the capsules were incubated in a simulated gastric fluid (SGF, pH = 2) or simulated intestinal fluid (SIF, pH = 7.4, both from RICCA Chemical). The fluid samples were stirred at room temperature. The release of DiD-labeled MΦ-NPs was quantified by measuring the DiD fluorescence signal (excitation/emission = 644/665 nm) in the fluid samples using a Tecan Infinite M200 plate reader (Tecan).

In Vitro Cytokine Binding Study. Recombinant mouse TNF-α (2 ng mL^{-1}), IL-1β (8 ng mL^{-1}), or IL-6 (8 ng mL^{-1}, all from Biolegend) was mixed with MΦ-NPs at final concentrations ranging from 0 to 2 mg mL^{-1}. The mixtures were incubated for 2 h at 37 °C, and the MΦ-NPs were removed by centrifugation at 16,100g for 10 min. The concentrations of unbound cytokines remaining in the supernatant were quantified using mouse TNF-α, IL-1β, and IL-6 enzyme-linked immunosorbent assays (ELISA, kits purchased from Biolegend). The measurements were carried out in 1× PBS (pH = 7.4). The bound cytokine levels were calculated by subtracting the concentration of unbound cytokines from the initial cytokine input. Nonlinear curve fitting was performed in GraphPad Prism 9.

Animals. All mice used in this study were housed in an animal facility at the University of California San Diego (UCSD) under federal, state, local, and National Institutes of Health (NIH) guidelines. 6-week-old male C57BL/6 mice were purchased from Jackson Laboratory and were maintained under standard housing with 12 h light−12 h dark cycle, ambient temperature, and average humidity. All animal experiments were performed in accordance with NIH guidelines and were approved by the Institutional Animal Care and Use Committee (IACUC) of UCSD.

Pharmacokinetics and Biodistribution Studies. Capsules loaded with DiR-labeled MΦ-NPs (3 mg per capsule) were orally administrated to 7-week-old male C57BL/6 mice using a capsule dosing syringe (Braintree Scientific). At 2, 4, 6, 10, and 24 h after oral gavage, three mice were euthanized at each time point, and the entire gastrointestinal (GI) tract was collected. The GI tracks were rinsed with 1× PBS three times for biodistribution analysis and imaged using a Xenogen IVIS 200 system. The collected GI tracks were weighed and homogenized for quantitative analysis in 1 mL of 1× PBS. The fluorescent signals were quantified using a Tecan Infinite M200 plate reader (Tecan, excitation/emission = 748/780 nm).

Dextran Sulfate Sodium (DSS)-Induced Mouse Colitis Model. Six-week-old male C57BL/6 mice were divided into groups of five mice per cage and acclimatized for 1 week before the in vivo experiments. In all studies, the nanosponge dosage was limited to a single capsule per day with its maximum nanosponge loading capacity. In a prophylactic regimen, the treatment started from day 1 and ended on day 9. Specifically, mice were administered with 3% DSS supplemented in drinking water for 6 days, followed by regular water. Mice fed with regular drinking water were used as a control group. During the treatment period, PBS, empty capsules, capsules loaded with RBC-NPs (denoted "cp-RBC-NPs", 3 mg of RBC-NPs per capsule), and capsules loaded with MΦ-NPs (denoted "cp-MΦ-NPs", 3 mg of MΦ-NPs per capsule) were orally administrated into mice using a capsule dosing syringe one capsule per day for 9 days. For the delayed treatment regimen, mice were administered 3% DSS supplemented in drinking water for 6 days, followed by regular drinking water. At the end of day 6, mice were orally administered with PBS, empty capsules, RBC-NP capsules (3 mg of RBC-NPs per capsule), and MΦ-NP capsules (3 mg of MΦ-NPs per capsule) at a dosage of one capsule per day until day 13.

Disease Severity via Body Weight, Fecal Samples, and Colon Length. In all studies, changes in the body weights of all mice were recorded daily throughout the experimental period. In addition, fecal samples were collected on predetermined time points used to calculate the disease activity index (DAI) based on stool consistency (0−4), rectal bleeding (0−4), and weight loss (0−4).[47] Specifically, (a) stool consistency: 0 = normal, 1 = soft stool, 2 = loose stool, and 4 = diarrhea; (b) rectal bleeding: 0 = no blood, 1 = Hemoccult positive, 2 = Hemoccult positive and visual pellet bleeding, and 4 = gross bleeding with blood around the anus; (c) weight loss: 0 = no loss, 1 = 1−5% loss, 2 = 5−10% loss, 3 = 10−20%, and 4 ≥ 20% loss. At the study end points, mice were euthanized. The entire colon was extracted, and the length was measured. Then, a piece of colonic tissue (0.5 cm in length, n = 5) was excised from the distal section and cut into three sections. The three sections were used for histological analysis, immunofluorescence staining, and mRNA quantification, respectively. The remaining colonic tissue was weighed and homogenized in 0.5 mL of 1× PBS for the quantification of pro-inflammatory cytokines concentration. In the quantification, homogenized samples were centrifuged for 10 min at 10,000g at 4 °C. The concentrations of TNF-α, IL-1β, and IL-6 in the supernatant were quantified using an ELISA kit (BioLegend).

Histological Analysis of Colonic Tissues. Colon samples collected from the above study were also used for H&E and TUNEL staining (n = 5, UCSD Histology Core). To quantify TUNEL positivity, five random areas were selected from each group. Within each area, the total number of cells and the number of TUNEL-positive cells were counted. TUNEL positivity was determined by calculating the ratio of TUNEL-positive cells to the total cells. For evaluating the disease severity, the histological samples were scored for the presence of neutrophilic and mononuclear infiltrates (0−3), epithelial architecture damage (0−3), muscle thickening (0−3), goblet cell depletion (0−1), and crypt abscess (0−1).[48] The colonic histological damage scores were summed, resulting in a final score between 0 and 11.

Immunofluorescence Microscopic Analysis of Colonic Tissues. For immunofluorescence analysis of ZO-1 and occludin-1 expressions on mouse colonic tissues, 0.5 cm of colonic tissues were fixed in Tissue-Tek O.C.T. Compound at −80 °C (Sakura Finetek). After cryosection, the colonic tissue samples were permeabilized with 0.25% Trition-100X and blocked with 2% bovine serum albumin (BSA) in 1× PBS for 1 h. The sections were then stained with 5 μg mL^{-1} mouse anti-ZO-1 antibodies conjugated with AlexaFluor-488 (ThermoFisher) and 1 μg mL^{-1} mouse antioccludin antibodies conjugated with AlexaFluor-594 (ThermoFisher) overnight at 4 °C. Meanwhile, Hoechst 33342 (1 μg mL^{-1}, ThermoFisher) was used for nuclei staining. Finally, the immunofluorescence signals were observed by using a confocal microscope (Leica SP8).

Quantitative Reverse Transcription PCR (qRT-PCR). According to the manufacturer's protocol, RNA was extracted from mouse colonic tissues using a Direct-zol RNA Miniprep kit (Zymo Research). The RNA was reverse transcribed into cDNA using the ProtoScript First Strand cDNA Synthesis kit (New England BioLabs), followed by qPCR using a LUNA Universal qPCR Master Mix (New England BioLabs). The cycling conditions were 95 °C for 1 min and then 40 cycles of 95 °C for 15 s and 60 °C for 45 s. The relative expression of target genes was calculated by using β-actin as a reference gene. The primers used for amplification include the following: ZO-1 forward (CTTCTCTTGCTGGCCCTAAAC), ZO-1 reverse (TGGCTTCACTTGAGGTTTCTG), Occludin forward (CACACTTGCTTGGGACAGAG), Occludin reverse (TAGCCATAGCCTCCATAGCC), β-actin forward (AAGTGTGACGTTGACATCCG), and β-actin reverse (GATCCACATCTGCTGGAAGG). All sequences refer to 5′ to 3′.

In Vivo Biosafety Study. For in vivo biosafety study, six-week-old male C57BL/6 mice were divided into groups of three mice per cage and acclimatized for 1 week before the in vivo experiments. During the study period, PBS (100 μL), empty capsules, and MΦ-NP

https://doi.org/10.1021/acsnano.3c03959
ACS Nano 2023, 17, 15893−15904

capsules (3 mg MΦ-NPs per capsule) were orally administrated into mice using a capsule dosing syringe at a dosage of one capsule per day for 7 days. Throughout the study, mouse weight changes were recorded daily, and the mice were euthanized at the end point for sample collection. For blood chemistry analysis and blood cell counts, mouse whole blood was collected into potassium−EDTA collection tubes (Sarstedt). The analysis was performed by the UCSD Animal Care Program Diagnostic Services Laboratory. For the histological analysis, the colons were sectioned and stained with H&E (Leica Biosystems), followed by imaging with a Nanozoomer 2.0-HT slide scanning system (Hamamatsu).

Microbiome Analysis. 200 mg amount of feces was collected from each mouse on day 8 of the in vivo biosafety study. The fecal samples were properly packed and shipped to Zymo Research Corporation for microbiome analysis. In brief, microbiome DNA was extracted from the mouse feces using a ZymoBIOMICS-96 MagBead DNA Kit. The isolated DNA was then used to generate 16S rRNA libraries via the Quick-16S NGS Library Prep Kit (all from Zymo Research). 16S rRNA sequencing was performed on Illumina MiSeq with a primer set specific to the V3 and V4 regions, and the analysis was conducted using Qiime v.1.9.1 and LEfSe analysis package.

ASSOCIATED CONTENT

Supporting Information

The Supporting Information is available free of charge at https://pubs.acs.org/doi/10.1021/acsnano.3c03959.

Capsule loading efficiency (Figure S1); morphology of freshly prepared MΦ-NPs (Figure S2); nanosponge colloidal stability (Figure S3); Western blot analysis of characteristic proteins on MΦ-NPs (Figure S4); cp-MΦ-NPs ameliorating inflammatory effects on cellular levels (Figure S5); in vitro cytotoxicity of cp-MΦ-NPs (Figure S6); scoring criteria of IBD disease activity index (Table S1) (PDF)

AUTHOR INFORMATION

Corresponding Authors

Weiwei Gao − *Department of Nanoengineering, Chemical Engineering Program, and Moores Cancer Center, University of California San Diego, La Jolla, California 92093, United States;* orcid.org/0000-0001-5196-4887; Email: w5gao@ucsd.edu

Liangfang Zhang − *Department of Nanoengineering, Chemical Engineering Program, and Moores Cancer Center, University of California San Diego, La Jolla, California 92093, United States;* orcid.org/0000-0003-0637-0654; Email: zhang@ucsd.edu

Authors

Yaou Duan − *Department of Nanoengineering, Chemical Engineering Program, and Moores Cancer Center, University of California San Diego, La Jolla, California 92093, United States*

Edward Zhang − *Department of Nanoengineering, Chemical Engineering Program, and Moores Cancer Center, University of California San Diego, La Jolla, California 92093, United States*

Ronnie H. Fang − *Department of Nanoengineering, Chemical Engineering Program, and Moores Cancer Center, University of California San Diego, La Jolla, California 92093, United States;* orcid.org/0000-0001-6373-3189

Complete contact information is available at: https://pubs.acs.org/10.1021/acsnano.3c03959

Notes

The authors declare no competing financial interest.

ACKNOWLEDGMENTS

This work is supported by the Defense Threat Reduction Agency Joint Science and Technology Office for Chemical and Biological Defense under Grant Number HDTRA1-21-1-0010. We thank Dr. Lee Swanson for the assistance for IBD animal model development.

REFERENCES

(1) Ng, S. C.; Shi, H. Y.; Hamidi, N.; Underwood, F. E.; Tang, W.; Benchimol, E. I.; Panaccione, R.; Ghosh, S.; Wu, J. C. Y.; Chan, F. K. L.; Sung, J. J. Y.; Kaplan, G. G. Worldwide incidence and prevalence of inflammatory bowel disease in the 21st century: a systematic review of population-based studies. *Lancet* **2017**, *390*, 2769−2778.

(2) Turner, J. R. Intestinal mucosal barrier function in health and disease. *Nat. Rev. Immunol.* **2009**, *9*, 799−809.

(3) Mehandru, S.; Colombel, J. F. The intestinal barrier, an arbitrator turned provocateur in IBD. *Nat. Rev. Gastro. Hepat.* **2021**, *18*, 83−84.

(4) Halfvarson, J.; Brislawn, C. J.; Lamendella, R.; Vazquez-Baeza, Y.; Walters, W. A.; Bramer, L. M.; D'Amato, M.; Bonfiglio, F.; McDonald, D.; Gonzalez, A.; McClure, E. E.; Dunklebarger, M. F.; Knight, R.; Jansson, J. K. Dynamics of the human gut microbiome in inflammatory bowel disease. *Nat. Microbiol.* **2017**, *2*, 17004.

(5) Franzosa, E. A.; Sirota-Madi, A.; Avila-Pacheco, J.; Fornelos, N.; Haiser, H. J.; Reinker, S.; Vatanen, T.; Hall, A. B.; Mallick, H.; McIver, L. J.; Sauk, J. S.; Wilson, R. G.; Stevens, B. W.; Scott, J. M.; Pierce, K.; Deik, A. A.; Bullock, K.; Imhann, F.; Porter, J. A.; Zhernakova, A.; et al. Gut microbiome structure and metabolic activity in inflammatory bowel disease. *Nat. Microbiol.* **2019**, *4*, 898.

(6) Alatab, S.; Sepanlou, S. G.; Ikuta, K.; Vahedi, H.; Bisignano, C.; Safiri, S.; Sadeghi, A.; Nixon, M. R.; Abdoli, A.; Abolhassani, H.; Alipour, V.; Almadi, M. A. H.; Almasi-Hashiani, A.; Anushiravani, A.; Arabloo, J.; Atique, S.; Awasthi, A.; Badawi, A.; Baig, A. A. A.; Bhala, N.; et al. The global, regional, and national burden of inflammatory bowel disease in 195 countries and territories, 1990−2017: a systematic analysis for the Global Burden of Disease Study 2017. *Lancet Gastroenterol.* **2020**, *5*, 17−30.

(7) Beard, J. A.; Franco, D. L.; Click, B. H. The burden of cost in inflammatory bowel disease: a medical economic perspective and the future of value-based care. *Curr. Gastroenterol. Rep.* **2020**, *22*, 6.

(8) Zhou, J.; Li, M. Y.; Chen, Q. F.; Li, X. J.; Chen, L. F.; Dong, Z. L.; Zhu, W. J.; Yang, Y.; Liu, Z.; Chen, Q. Programmable probiotics modulate inflammation and gut microbiota for inflammatory bowel disease treatment after effective oral delivery. *Nat. Commun.* **2022**, *13*, 3432.

(9) Bernstein, C. N.; Fried, M.; Krabshuis, J. H.; Cohen, H.; Eliakim, R.; Fedail, S.; Gearry, R.; Goh, K. L.; Hamid, S.; Khan, A. G.; LeMair, A. W.; Malfertheiner; Qin, O. Y.; Rey, J. F.; Sood, A.; Steinwurz, F.; Thomsen, O. O.; Thomson, A.; Watermeyer, G. World gastroenterology organization practice guidelines for the diagnosis and management of IBD in 2010. *Inflamm. Bowel Dis.* **2010**, *16*, 112−124.

(10) Bressler, B.; Marshall, J. K.; Bernstein, C. N.; Bitton, A.; Jones, J.; Leontiadis, G. I.; Panaccione, R.; Steinhart, A. H.; Tse, F.; Feagan, B.; Colitis, T. U.; et al. Clinical practice guidelines for the medical management of nonhospitalized ulcerative colitis: The Toronto Consensus. *Gastroenterology* **2015**, *148*, 1035−1529.

(11) Hansel, T. T.; Kropshofer, H.; Singer, T.; Mitchell, J. A.; George, A. J. T. The safety and side effects of monoclonal antibodies. *Nat. Rev. Drug Discovery* **2010**, *9*, 325−338.

(12) Sathish, J. G.; Sethu, S.; Bielsky, M. C.; de Haan, L.; French, N. S.; Govindappa, K.; Green, J.; Griffiths, C. E. M.; Holgate, S.; Jones, D.; Kimber, I.; Moggs, J.; Naisbitt, D. J.; Pirmohamed, M.; Reichmann, G.; Sims, J.; Subramanyam, M.; Todd, M. D.; Van der Laan, J. W.; Weaver, R. J.; et al. Challenges and approaches for the

development of safer immunomodulatory biologics. *Nat. Rev. Drug Discovery* **2013**, *12*, 306−324.
(13) Li, D. F.; Yang, M. F.; Xu, H. M.; Zhu, M. Z.; Zhang, Y.; Tian, C. M.; Nie, Y. Q.; Wang, J. Y.; Liang, Y. J.; Yao, J.; Wang, L. S. Nanoparticles for oral delivery: targeted therapy for inflammatory bowel disease. *J. Mater. Chem. B* **2022**, *10*, 5853−5872.
(14) Xiao, B.; Laroui, H.; Viennois, E.; Ayyadurai, S.; Charania, M. A.; Zhang, Y. C.; Zhang, Z.; Baker, M. T.; Zhang, B. Y.; Gewirtz, A. T.; Merlin, D. Nanoparticles with surface antibody against CD98 and carrying CD98 small interfering RNA reduce colitis in mice. *Gastroenterology* **2014**, *146*, 1289−1300.
(15) Xiao, B.; Laroui, H.; Ayyadurai, S.; Viennois, E.; Charania, M. A.; Zhang, Y. C.; Merlin, D. Mannosylated bioreducible nanoparticle-mediated macrophage-specific TNF-alpha RNA interference for IBD therapy. *Biomaterials* **2013**, *34*, 7471−7482.
(16) Gou, S. Q.; Huang, Y. M.; Wan, Y.; Ma, Y.; Zhou, X.; Tong, X. L.; Huang, J.; Kang, Y. J.; Pan, G. Q.; Dai, F. Y.; Xiao, B. Multi-bioresponsive silk fibroin-based nanoparticles with on-demand cytoplasmic drug release capacity for CD44-targeted alleviation of ulcerative colitis. *Biomaterials* **2019**, *212*, 39−54.
(17) Ali, H.; Weigmann, B.; Neurath, M. F.; Collnot, E. M.; Windbergs, M.; Lehr, C. M. Budesonide loaded nanoparticles with pH-sensitive coating for improved mucosal targeting in mouse models of inflammatory bowel diseases. *J. Controlled Release* **2014**, *183*, 167−177.
(18) Wilson, D. S.; Dalmasso, G.; Wang, L. X.; Sitaraman, S. V.; Merlin, D.; Murthy, N. Orally delivered thioketal nanoparticles loaded with TNF-alpha-siRNA target inflammation and inhibit gene expression in the intestines. *Nat. Mater.* **2010**, *9*, 923−928.
(19) Yan, X. J.; Pan, Q.; Xin, H. H.; Chen, Y. X.; Ping, Y. Genome-editing prodrug: Targeted delivery and conditional stabilization of CRISPR-Cas9 for precision therapy of inflammatory disease. *Sci. Adv.* **2021**, *7*, No. eabj0624.
(20) Wang, X. Y.; Yan, J. J.; Wang, L. Z.; Pan, D. H.; Xu, Y. P.; Wang, F.; Sheng, J.; Li, X. N.; Yang, M. Oral delivery of anti-TNF antibody shielded by natural polyphenol-mediated supramolecular assembly for inflammatory bowel disease therapy. *Theranostics* **2020**, *10*, 10808−10822.
(21) Lee, Y.; Sugihara, K.; Gillilland, M. G.; Jon, S.; Kamada, N.; Moon, J. J. Hyaluronic acid-bilirubin nanomedicine for targeted modulation of dysregulated intestinal barrier, microbiome and immune responses in colitis. *Nat. Mater.* **2020**, *19*, 118−126.
(22) Liu, H.; Cai, Z. W.; Wang, F.; Hong, L. W.; Deng, L. F.; Zhong, J.; Wang, Z. T.; Cui, W. G. Colon-targeted adhesive hydrogel microsphere for regulation of gut immunity and flora. *Adv. Sci.* **2021**, *8*, No. 2101619.
(23) Liu, Y. F.; Cheng, Y.; Zhang, H.; Zhou, M.; Yu, Y. J.; Lin, S. C.; Jiang, B.; Zhao, X. Z.; Miao, L. Y.; Wei, C. W.; Liu, Q. Y.; Lin, Y. W.; Du, Y.; Butch, C. J.; Wei, H. Integrated cascade nanozyme catalyzes in vivo ROS scavenging for anti-inflammatory therapy. *Sci. Adv.* **2020**, *6*, No. eabb2695.
(24) Wang, D.; Wang, S. Y.; Zhou, Z. D.; Bai, D.; Zhang, Q. Z.; Ai, X. Z.; Gao, W.; Zhang, L. White Blood Cell Membrane-Coated Nanoparticles: Recent Development and Medical Applications. *Adv. Healthc. Mater.* **2022**, *11*, No. 2101349.
(25) Thamphiwatana, S.; Angsantikul, P.; Escajadillo, T.; Zhang, Q. Z.; Olson, J.; Luk, B. T.; Zhang, S.; Fang, R. H.; Gao, W.; Nizet, V.; Zhang, L. Macrophage-like nanoparticles concurrently absorbing endotoxins and proinflammatory cytokines for sepsis management. *Proc. Natl. Acad. Sci. U.S.A.* **2017**, *114*, 11488−11493.
(26) Zhang, Q. Z.; Zhou, J. L.; Zhou, J. R.; Fang, R. H.; Gao, W.; Zhang, L. Lure-and-kill macrophage nanoparticles alleviate the severity of experimental acute pancreatitis. *Nat. Commun.* **2021**, *12*, 4136.
(27) Hou, M. Y.; Wei, Y. S.; Zhao, Z. Y.; Han, W. Q.; Zhou, R. X.; Zhou, Y.; Zheng, Y. R.; Yin, L. C. Immuno-engineered nanodecoys for the multi-target anti-inflammatory treatment of autoimmune diseases. *Adv. Mater.* **2022**, *34*, No. 2108817.
(28) Wei, X. L.; Zhang, G.; Ran, D. N.; Krishnan, N.; Fang, R. H.; Gao, W.; Spector, S. A.; Zhang, L. T-cell-mimicking nanoparticles can neutralize HIV infectivity. *Adv. Mater.* **2018**, *30*, No. 1802233.
(29) Na, Y. R.; Stakenborg, M.; Seok, S. H.; Matteoli, G. Macrophages in intestinal inflammation and resolution: a potential therapeutic target in IBD. *Nat. Rev. Gastro. Hepat.* **2019**, *16*, 531−543.
(30) Bandi, S. P.; Kumbhar, Y. S.; Venuganti, V. V. K. Effect of particle size and surface charge of nanoparticles in penetration through intestinal mucus barrier. *J. Nanoparticle Res.* **2020**, *22*, 62.
(31) Hu, C. M. J.; Fang, R. H.; Copp, J.; Luk, B. T.; Zhang, L. A biomimetic nanosponge that absorbs pore-forming toxins. *Nat. Nanotechnol.* **2013**, *8*, 336−340.
(32) Hu, C. M. J.; Fang, R. H.; Wang, K. C.; Luk, B. T.; Thamphiwatana, S.; Dehaini, D.; Nguyen, P.; Angsantikul, P.; Wen, C. H.; Kroll, A. V.; Carpenter, C.; Ramesh, M.; Qu, V.; Patel, S. H.; Zhu, J.; Shi, W.; Hofman, F. M.; Chen, T. C.; Gao, W.; Zhang, K.; et al. Nanoparticle biointerfacing by platelet membrane cloaking. *Nature* **2015**, *526*, 118−121.
(33) El-Maghawry, E.; Tadros, M. I.; Elkheshen, S. A.; Abd-Elbary, A. Eudragit (R)-S100 Coated PLGA Nanoparticles for Colon Targeting of Etoricoxib: Optimization and Pharmacokinetic Assessments in Healthy Human Volunteers. *Int. J. Nanomedicine* **2020**, *15*, 3965−3980.
(34) Zhang, Q. Z.; Honko, A.; Zhou, J. R.; Gong, H.; Downs, S. N.; Vasquez, J. H.; Fang, R. H.; Gao, W.; Griffiths, A.; Zhang, L. Cellular nanosponges inhibit SARS-CoV-2 infectivity. *Nano Lett.* **2020**, *20*, 5570−5574.
(35) Neurath, M. F. Cytokines in inflammatory bowel disease. *Nat. Rev. Immunol.* **2014**, *14*, 329−342.
(36) Swanson, L.; Katkar, G. D.; Tam, J.; Pranadinata, R. F.; Chareddy, Y.; Coates, J.; Anandachar, M. S.; Castillo, V.; Olson, J.; Nizet, V.; Kufareva, I.; Das, S.; Ghosh, P. TLR4 signaling and macrophage inflammatory responses are dampened by GIV/Girdin. *Proc. Natl. Acad. Sci. U.S.A.* **2020**, *117*, 26895−26906.
(37) Eichele, D. D.; Kharbanda, K. K. Dextran sodium sulfate colitis murine model: An indispensable tool for advancing our understanding of inflammatory bowel diseases pathogenesis. *World J. Gastroentero.* **2017**, *23*, 6016−6029.
(38) Arda-Pirincci, P.; Aykol-Celik, G. Galectin-1 reduces the severity of dextran sulfate sodium (DSS)-induced ulcerative colitis by suppressing inflammatory and oxidative stress response. *Bosn. J. Basic Med. Sci.* **2019**, *20*, 319−328.
(39) Araki, Y.; Bamba, T.; Mukaisho, K. I.; Kanauchi, O.; Ban, H.; Bamba, S.; Andoh, A.; Fujiyama, Y.; Hattori, T.; Sugihara, H. Dextran sulfate sodium administered orally is depolymerized in the stomach and induces cell cycle arrest plus apoptosis in the colon in early mouse colitis. *Oncol. Rep.* **2012**, *28*, 1597−1605.
(40) Fang, R. H.; Kroll, A. V.; Gao, W.; Zhang, L. Cell membrane coating nanotechnology. *Adv. Mater.* **2018**, *30*, No. 1706759.
(41) Wang, S. Y.; Wang, D.; Duan, Y. O.; Zhou, Z. D.; Gao, W. W.; Zhang, L. Cellular Nanosponges for Biological Neutralization. *Adv. Mater.* **2022**, *34*, No. 2107719.
(42) Lamprecht, A. IBD Selective nanoparticle adhesion can enhance colitis therapy. *Nat. Rev. Gastro. Hepat.* **2010**, *7*, 311−312.
(43) Zhang, Y. C.; Si, X. M.; Yang, L.; Wang, H.; Sun, Y.; Liu, N. Association between intestinal microbiota and inflammatory bowel disease. *Animal Model Exp. Med.* **2022**, *5*, 311−322.
(44) Ni, J.; Wu, G. D.; Albenberg, L.; Tomov, V. T. Gut microbiota and IBD: causation or correlation? *Nat. Rev. Gastro. Hepat.* **2017**, *14*, 573−584.
(45) Zhang, Q.; Fang, R.; Gao, W.; Zhang, L. A biomimetic nanoparticle to 'lure and kill' phospholipase A2. *Angew. Chem., Int. Ed.* **2020**, *59*, 10461−10465.
(46) Chen, Y.; Zhang, Y.; Zhuang, J.; Lee, J. H.; Wang, L.; Fang, R.; Gao, W.; Zhang, L. Cell membrane-cloaked oil nanosponges enable dual-modal detoxification. *ACS Nano* **2019**, *13*, 7209−7215.
(47) Kim, J. J.; Shajib, M. S.; Manocha, M. M.; Khan, W. I. Investigating Intestinal Inflammation in DSS-induced Model of IBD. *J. Vis. Exp.* **2012**, 1−6.

https://doi.org/10.1021/acsnano.3c03959
ACS Nano 2023, 17, 15893−15904

(48) Das, S.; Sarkar, A.; Choudhury, S. S.; Owen, K. A.; Derr-Castillo, V. L.; Fox, S.; Eckmann, L.; Elliott, M. R.; Casanova, J. E.; Ernst, P. B. Engulfment and cell motility protein 1 (ELMO1) has an essential role in the internalization of Salmonella typhimurium into enteric macrophages that impact disease outcome. *Cell Mol. Gastroenter.* **2015**, *1*, 311−324.

https://doi.org/10.1021/acsnano.3c03959
ACS Nano 2023, 17, 15893−15904